

Ultrafast Magnetoelastic Probing of Surface Acoustic Transients

J. Janušonis,^{1,*} C.L. Chang,^{1,*} T. Jansma,¹ A. Gatilova,¹ A.M. Lomonosov,²
V. Shalagatskyi,² V.S. Vlasov,² V.V. Temnov,^{2,3} and R.I. Tobey^{1,†}

¹*Zernike Institute for Advanced Materials, University of Groningen, Groningen, The Netherlands*

²*IMMM CNRS 6283, Université du Maine, 72085 Le Mans cedex, France*

³*Fritz-Haber-Institut der Max-Planck-Gesellschaft,*

Abteilung Physikalische Chemie, Faradayweg 4-6, 14195 Berlin, Germany

We generate in-plane magnetoelastic waves in nickel films using the all-optical transient grating technique. When performed on amorphous glass substrates, two dominant magnetoelastic excitations can be resonantly driven by the underlying elastic distortions, the Rayleigh Surface Acoustic Wave and the Surface Skimming Longitudinal Wave. An applied field, oriented in the sample plane, selectively tunes the coupling between magnetic precession and one of the elastic waves, thus demonstrating selective excitation of coexisting, large amplitude magnetoelastic waves. Analytical calculations based on the Green's function approach corroborate the generation of the non-equilibrium surface acoustic transients.

PACS numbers:

Generating elementary excitations at solid surfaces and interfaces underscores many processes in materials and enhances their use in modern technology. With the increased emphasis on new materials and enhanced functionality of existing materials, generating and detecting multiple, competing excitations at the surface provides opportunities to expanded implementation. As many of these excitations are transient in nature, the use of ultra-short optical pulses provides for the generation and real-time monitoring of their dynamics, and allows for the time-domain identification of their effects on the state of the material¹.

The effects of competing excitations on material properties are exemplified in plasmonics. In research related to extraordinary transmission of light through sub-wavelength apertures²⁻⁴ a long-lasting controversy exists over the nature of the responsible mechanism. It is currently understood that two competing excitations, the so-called Composite Diffraction Evanescent Waves (CDEW) and the conventional Surface Plasmon Polaritons (SPPs), conspire to enhance transmission through apertures, while their contributions depend strongly on the experimental geometry. Alternatively, new model systems are sought in order to shed further light on extraordinary transmission effects, and acoustic analogues have been demonstrated⁵.

In this Letter we report on the generation and selective detection of two surface acoustic waves, which are analogous to CDEW and SPP in plasmonics. The combination of femtosecond transient grating (TG) excitation with ultrafast time-resolved magneto-optical spectroscopy allows for an unambiguous observation of Rayleigh Surface Acoustic Wave (SAW) and a short-living Surface Skimming Longitudinal Wave (SSLW), both of which couple to the magnetization of the material. The differences in the acoustic properties between SAW and SSLW provides the possibility to selectively probe the individual acoustic modes via the resonant magneto-elastic excitation, and represents an advantage when compared to the analogous

plasmonic investigations, particularly in regards to the selectivity in detection between the two competing excitations. The combination of novel experimental and analytical theoretical tools represents a powerful playground for the design of ultrafast magneto-optical and magneto-acoustic devices. As the most straight-forward application, our results can contribute to the detailed understanding of the extraordinary high acoustic transmission through the periodically microstructured surfaces, and by searching for novel phenomena in the magneto-optical transmission measurements through sub-wavelength hole arrays patterned in hybrid metal-ferromagnet multilayers. In a broader context, the knowledge of SAW and SSLW generation in complex nanostructures can help tailor the thermal transport through interfaces.

We recently demonstrated a novel excitation geometry for generating magnetoelastic waves, whereby narrowband planar elastic waves were shown to resonantly drive planar magnetization precession using Rayleigh type Surface Acoustic Waves. Using the Transient Grating geometry⁶⁻⁹, we were able to demonstrate frequency tunability from 1 GHz to ≈ 6 GHz. Here we demonstrate the broader utility of the TG technique for generating additional planar elastic waves, beyond Rayleigh SAW, which also drive magnetization precession. The TG geometry generates all elastic modes that satisfy the boundary condition imposed by the thermoelastic stress, regardless of frequency. Therefore, in our geometry we access additional elastic excitations known as Surface Skimming Longitudinal Waves. Under such excitation conditions, both elastic waves are excited simultaneously, and we show the magnetic field selective coupling of the magnetization precession to each elastic wave independently.

In the TG geometry, short pulses of light at 400 nm are crossed onto the sample surface, which upon superposition result in a spatially periodic excitation of the sample, as shown in Fig. 1. In this excitation geometry, all elastic modes that satisfy the elastic boundary conditions are excited at the wavevector $2\pi/\Lambda$ determined

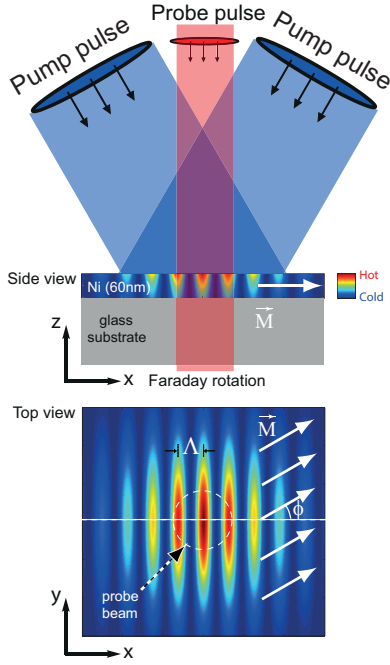


FIG. 1: Experimental geometry showing the thin nickel film with glass substrate. The transient grating is generated by two crossed femtosecond laser pump pulses, leading to a spatially-periodic impulsive heating of a thin nickel film and the launching of acoustic waves along the surface of the semi-infinite glass substrate. Grating periodicities as small as $1 \mu\text{m}$ can be achieved. A magnetic field can be rotated continuously in the sample plane. Faraday rotation of time-delayed optical probe pulses transmitted through the sample monitors the interaction between elastic and magnetic degrees of freedom.

by the crossing of two beams. Subsequent to the excitation, a time-delayed probe pulse impinges normally onto the sample surface and the transmitted radiation is polarization analyzed (Faraday detection). The sample is held in a magnetic field that can be swept continuously from -1.5 kG to $+1.5 \text{ kG}$ and rotated around the sample normal.

The samples under study are composed of thin polycrystalline nickel films on glass substrates (soda lime glass). Representative data showing the grating dependence of the Faraday response are shown in Fig. 2(a) for a film thickness of 60 nm . In contrast to our previous results⁷ which were reported for the nickel/MgO sample structure, when performing measurements on glass substrates additional dynamics can be observed. Cursory evaluation of the data in Fig. 2(a) shows that both oscillation amplitude and frequency reduce as the excitation grating period is increased, and eventually disappear when a single pump beam is used to excite the material. Secondly, the dynamics in the first nanosecond are comprised of a two oscillating contributions, which suggests the presence of two distinct magnetoelastic waves.

Assignment of the modes is accomplished by plotting the frequencies of both modes as a function of excitation

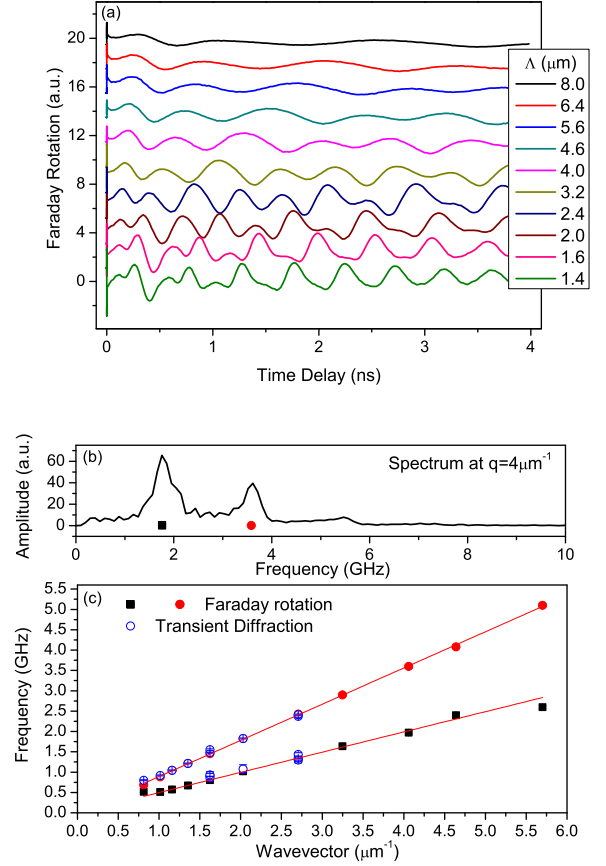


FIG. 2: (a) The time-resolved Faraday rotation measures the acoustically induced magnetization precession. As the period of the transient grating is increased, the precession decreases in frequency and amplitude. In the limit of a single pump beam excitation, the magnetic precession is completely suppressed. (c) The frequency of oscillation versus wavevector measures the velocity of acoustic propagation. Red and black data points represent frequencies extracted from (a), and blue data points are extracted from the nonmagnetic transient grating detection. Near perfect linear dependence allows us to identify two types of excitations as the Rayleigh Surface Acoustic Wave (lower branch) and the Surface Skimming Longitudinal Wave (upper branch) propagating at $3120 \pm 20 \text{ m/s}$ and $5590 \pm 15 \text{ m/s}$, respectively.

wavevector. In Fig. 2(b) we display the Fourier Transform of the zero field response showing two oscillations. For $\Lambda = 1.57 \mu\text{m}$, and correspondingly $k = 4 \mu\text{m}^{-1}$, the extracted frequencies are 1.75 GHz and 3.6 GHz , respectively. In Fig. 2(c) these frequencies are plotted for a range of applied grating periodicities. Overlaid onto the Faraday response are data acquired in the conventional transient grating geometry, where light is diffracted from acoustic waves (data not shown, see Ref.5 for details). Such an experimental scheme is known to be sensitive to the underlying elastic waves and their associated structural distortions. From the correspondence between the

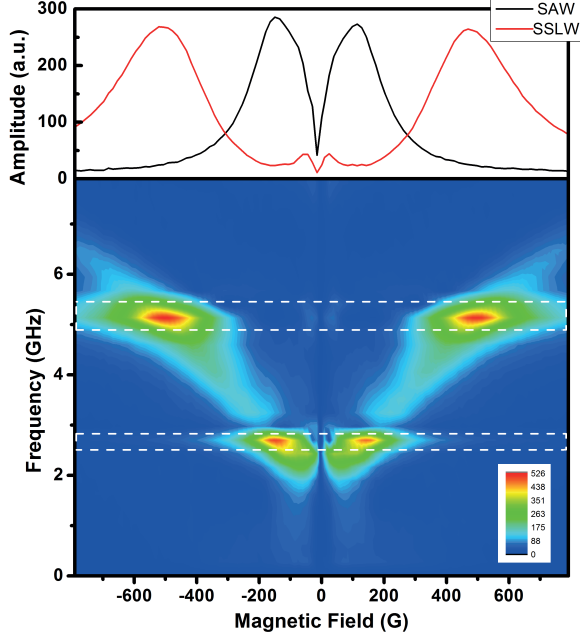


FIG. 3: Under appropriate field conditions the time-periodic effective magnetic field of the passing elastic wave resonantly couples to the precessional motion in the film, driving large amplitude precessional motion. For $\Lambda = 1.1 \mu\text{m}$, the upper frequency at 5.1 GHz is that of the SSLW while the lower frequency at 2.8 GHz corresponds to the SAW. In the upper panel, vertically-averaged signal within the indicated boxes for both SAW and SSLW is displayed.

two detection schemes, we are able to fit a single linear relationship (with zero intercept) providing the following mode assignments and their respective velocities: The lower branch propagates at $3120 \pm 20 \text{ m/s}$ which we assign as the Rayleigh Surface Acoustic Wave, the same excitation witnessed on MgO substrates⁷. In the long wavelength limit ($\Lambda > 1 \mu\text{m}$), the propagation velocity of the Rayleigh SAW in the Ni/substrate heterostructure is dictated by the substrate elastic constants due to the finite penetration depth ($\approx \Lambda \gg d_{Ni}$) of the elastic wave. This velocity compares favorably with the Rayleigh SAW velocity of the glass substrates, 3100 m/s for soda lime glass. The upper branch, propagating at a velocity of $5590 \pm 15 \text{ m/s}$, is the in-plane longitudinal acoustic wave, which has been termed previously as a Surface Skimming Longitudinal Wave (SSLW)¹⁰, or the Surface Skimming Bulk Wave (SSBW)¹¹, an elastic excitation that has been used extensively for non-destructive material evaluation^{12,13}. Again, the velocity is very close to the longitudinal sound velocity in glass (literature value 5400 m/s) due to the predominant concentration of elastic energy in the substrate.

We now discuss the effect of applying an in-plane magnetic field. As we had shown previously⁷, applying a magnetic field \vec{H}_{ext} in the plane of the sample provides

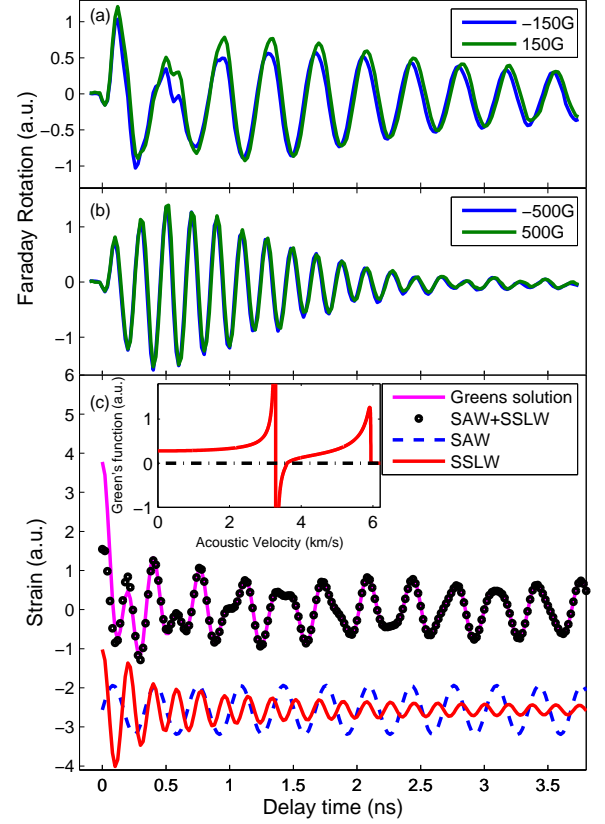


FIG. 4: Time traces at the resonances for (a) SAW and (b) SSLW, taken from Fig. 3(main panel). Switching the polarity of the magnetic field yields nearly identical oscillation amplitudes and phases which can be understood by considering the applied torque induced by magnetoelastic coupling. (c) The time-dependent strain $\epsilon_{xx}(t)$ calculated by Green's function formalism (discussed in the Supplemental Material) confirms the simultaneous excitation of SAW and SSLW modes. Whereas the decay of the acoustic eigenmode SAW is negligible, the amplitude of SLLW decreases as $1/t$, as expected for an acoustic diffraction phenomenon in a cylindric geometry.

the coupling between the elastic field at frequency v_{ac}/Λ and the ferromagnetic resonance of the film at frequency $f_{FMR} \propto \sqrt{H_{ext}(H_{ext} + M)}$. The magnitude H_{ext} of the applied field tunes the precessional FMR frequency of the film to match either SAW or SSLW frequency (M is the saturation magnetization of the thin magnetic film). The effect of having two elastic fields present, provides for the selective excitation of one magnetization precession response. A representative field scan is shown in Fig. 3(main panel, the Fourier Transform amplitude of the Faraday signal) for a grating period of $1.1 \mu\text{m}$ for both polarities of the applied field. The elastic frequencies at $\Lambda = 1.1 \mu\text{m}$ associated with SAW and SSLW are indicated by rectangles over the data, while lineouts of the vertically integrated values in the bounding boxes

are displayed in Fig. 3(top). As the applied field is tuned into resonance, the oscillation amplitude of the magnetization precession peaks, and then reduces as the field is tuned above resonance. For all applied fields, it should be recognized that two elastic waves are active, but the resonance condition drives a single precessional motion of the magnetization. The maxima occur at the location where the elastic driving frequency matches FMR frequency.

The temporal responses at the two resonant conditions, ± 150 G and ± 500 G, are shown in Fig. 4, exhibiting the same amplitude and phase of oscillation for both polarities of the magnetic field. The correspondence in oscillation phase for two directions of the magnetic field can be understood by considering the torque applied to the magnetization via the magnetoelastic coupling, through the Landau-Lifshits-Gilbert equation: $\partial \vec{M} / \partial t \propto \vec{M} \times [\vec{H}_{ext} + \vec{H}_{shape} + \vec{H}_{me}(t)]$, where the time-periodic effective field $\vec{H}_{me}(t)$ is determined by magnetoelastic interactions and can be calculated as a derivative of a the magneto-elastic term in the free energy density with respect to magnetization^{14,15}. The out-of-plane torque component originates from the coupling of in-plane longitudinal strain ($\epsilon_{xx}(t)$, the primary strain component in the SSLW and the dominant component in the SAW wave) and the in-plane components M_x and M_y of magnetization vector: $\partial \vec{M}_z / \partial t \propto \epsilon_{xx}(t) M_x M_y$. When the magnetization is inverted, i.e. $M_x \rightarrow -M_x$ and $M_y \rightarrow -M_y$, the magnetoelastic torque direction, and therefore the precessional direction, remains unchanged. On the contrary, if the magnetization is reflected with respect the acoustic wavevector ($M_x \rightarrow M_x$ and $M_y \rightarrow -M_y$, which is equivalent to $\phi \rightarrow -\phi$) the direction of magnetization precession changes in accordance with the above equation (Fig. 1S in the Supplemental Material). We note that the foregoing discussion on magnetoelasticity is related to a myriad of other ultra-fast work^{14,16–21} as well as it's connection to quasi-static 'straintronics'^{22,23}.

The differences in lifetime of the respective modes (Fig. 4(a),(b)) can be traced directly to the nature of the elastic driving field underscoring these effects. Whereas the SAW is a surface propagating elastic eigenwave with negligible energy dissipation, the SSLW is not a surface bound wave in this strict sense, and thus significant elastic energy propagates away from the active magnetic layer. Thus the strain amplitude of this higher frequency mode decays rapidly as elastic energy leaks away from the magnetically active material.

Qualitatively similar results can be found by solving the Green's Function response of an elastic half space, which at present we consider to be free of the bounding magnetic film²⁴. Convolution of the impulse response with spatially periodic stress associated with Λ results in a series of elastic excitations, most notably the SAW and SSLW that reside along the surface of the sample. The results of such a calculation (discussed in more de-

tail in the Supplemental Material) are displayed in figure Fig. 4(c). The time evolution for the strain amplitude can be robustly reproduced by assuming independent elastic waves (SAW and SSLW), while there sum shows excellent correspondence with the Green's function result. The two elastic constituents are assumed to be the negligibly decaying SAW and highly damped SSLW, which decays with 1/time dependency in accordance with the cylindrical symmetry of the grating excitation. Thus, both experiment and theory corroborate the coexistence of elastic waves, while field tuning allows us to monitor each wave independently through it's magnetoelastic coupling.

Finally, we note that measurements performed in similar planar geometries using elastic transducers to generate elastic waves and drive magnetic precession^{25–28} do not witness similar SSLW excitations. In the TG geometry, we launch all elastic modes which satisfy the boundary conditions imposed by the spatially periodic stress conditions. The transducer measurements additionally control the driving frequency, and thus primarily excite the SAW excitation only. Furthermore, as evident from our time traces, the SSLW excitations at multi-GHz frequencies experience far larger decay rates than SAW and thus would inhibit their detection in a non-local geometry based on generation and detection transducers that are spatially separated. In our local measurements, where the excitation and detection are performed in the same position, enhance the detection of such short lived elastic waves.

In summary, we have demonstrated the generation of two distinct elastic waves using a single excitation geometry, based on the transient grating technique. The two modes are identified as the surface-bound Rayleigh Surface Acoustic Wave (SAW) and the leaky Surface Skimming Longitudinal Wave (SSLW). Both elastic excitations couple to and drive the magnetization precession in a resonant fashion when an appropriate magnetic field is applied. Furthermore, since both elastic distortions are active simultaneously, we demonstrated the field tuned selectivity of each magnetoelastic excitation. The current measurements are distinguished by their time-domain approach which allowed us to witness the coupling between acoustic and magnetic degrees of freedom in real time. We envisage further experimental efforts to focus on extraordinary transmission of acoustic waves through sub-wavelength apertures while the magnetoelastic detection scheme provides for individual sensitivity to both elastic wave effects, opening possibilities to study competition between different elastic contributions to transmission measurements.

Authors thank K. A. Nelson, A.A. Maznev, and J.Y. Duquesne for discussions. We thank M. de Roos for assistance with e-beam sample preparation. Funding from Nouvelle équipe, nouvelle thématique et Stratégie internationale NNN-Telecom de la Région Pays de La Loire, Russian Foundation for Basic Research (Grant No. 15-02-07575) and Alexander von Humboldt Stiftung is grate-

fully acknowledged.

-
- * These authors contributed equally
[†] Electronic address: r.i.tobey@rug.nl
- ¹ V. V. Temnov, *Nature Photonics* **6**, 728 (2012).
 - ² T. Ebbesen, H. Lezec, H. Ghaemi, T. Thio, and P. Wolff, *Nature* **391**, 667 (1998).
 - ³ H. Lezec and T. Thio, *Optics Express* **12**, 3629 (2004).
 - ⁴ G. Gay, O. Alloschery, B. De Lesegno, C. O'Dwyer, J. Weiner, and H. Lezec, *Nature Physics* **2**, 262 (2006).
 - ⁵ M.-H. Lu, X.-K. Liu, L. Feng, J. Li, C.-P. Huang, and Y.-F. Chen, *Physical Review Letters* **99**, 174301 (2007).
 - ⁶ J. Rogers, A. Maznev, M. Banet, and K. Nelson, *Annual Review of Material Science* **30**, 117 (2000).
 - ⁷ J. Janusonis, C. L. Chang, P. H. M. van Loosdrecht, and R. I. Tobey, *Applied Physics Letters* **106**, 181601 (2015).
 - ⁸ J. D. Koralek, C. P. Weber, J. Orenstein, B. A. Bernevig, S.-C. Zhang, S. Mack, and D. D. Awschalom, *Nature* **458**, 610 (2009).
 - ⁹ R. I. Tobey, M. E. Siemens, M. M. Murnane, H. C. Kapteyn, D. H. Torchinsky, and K. A. Nelson, *Applied Physics Letters* **89**, 091108 (2006).
 - ¹⁰ B. Xu, Z. Shen, X. Ni, and J. Lu, *Journal of Applied Physics* **95**, 2116 (2004).
 - ¹¹ M. Lewis, *IEEE Transactions on Sonics and Ultrasonics* **25**, 256 (1978).
 - ¹² S. Sathish, R. Martin, and T. Moran, *Journal of the Acoustical Society of America* **115**, 165 (2004).
 - ¹³ A. Abbas, Y. Guillet, J. M. Rampnoux, P. Rigail, E. Motay, B. Audoin, and S. Dilhaire, *Optics Express* **22**, 7831 (2014).
 - ¹⁴ O. Kovalenko, T. Pezeril, and V. V. Temnov, *Physical Review Letters* **110**, 266602 (2013).
 - ¹⁵ L. Dreher, M. Weiler, M. Pernpeintner, H. Huebl, R. Gross, M. S. Brandt, and S. T. B. Goennenwein, *Physical Review B* **86**, 134415 (2012).
 - ¹⁶ A. V. Scherbakov, A. S. Salasyuk, A. V. Akimov, X. Liu, M. Bombeck, C. Brueggemann, D. R. Yakovlev, V. F. Sapega, J. K. Furdyna, and M. Bayer, *Physical Review Letters* **105**, 117204 (2010).
 - ¹⁷ T. L. Linnik, A. V. Scherbakov, D. R. Yakovlev, X. Liu, J. K. Furdyna, and M. Bayer, *Physical Review B* **84**, 214432 (2011).
 - ¹⁸ M. Bombeck, J. V. Jaeger, A. V. Scherbakov, T. Linnik, D. R. Yakovlev, X. Liu, J. K. Furdyna, A. V. Akimov, and M. Bayer, *Physical Review B* **87**, 060302 (2013).
 - ¹⁹ J.-W. Kim, M. Vomir, and J.-Y. Bigot, *Physical Review Letters* **109**, 166601 (2012).
 - ²⁰ J. V. Jaeger, A. V. Scherbakov, T. L. Linnik, D. R. Yakovlev, M. Wang, P. Wadley, V. Holy, S. A. Cavill, A. V. Akimov, A. W. Rushforth, et al., *Applied Physics Letters* **103**, 032409 (2013).
 - ²¹ J. V. Jaeger, A. V. Scherbakov, B. A. Glavin, A. S. Salasyuk, R. P. Campion, A. W. Rushforth, D. R. Yakovlev, A. V. Akimov, and M. Bayer, *Physical Review B* **92**, 020404 (2015).
 - ²² K. Roy, S. Bandyopadhyay, and J. Atulasimha, *Applied Physics Letters* **99**, 063108 (2011).
 - ²³ L. Thevenard, J. Y. Duquesne, E. Peronne, H. J. von Bardeleben, H. Jaffres, S. Ruttala, J.-M. George, A. Lemaitre, and C. Gourdon, *Physical Review B* **87**, 144402 (2013).
 - ²⁴ D. Lee, *IEEE Transactions on Sonics and Ultrasonics* **27**, 77 (1980).
 - ²⁵ S. Davis, A. Baruth, and S. Adenwalla, *Applied Physics Letters* **97**, 232507 (2010).
 - ²⁶ L. Thevenard, C. Gourdon, J. Y. Prieur, H. J. von Bardeleben, S. Vincent, L. Becerra, L. Largeau, and J. Y. Duquesne, *Physical Review B* **90**, 094401 (2014).
 - ²⁷ M. Weiler, L. Dreher, C. Heeg, H. Huebl, R. Gross, M. S. Brandt, and S. T. B. Goennenwein, *Physical Review Letters* **106**, 117601 (2011).
 - ²⁸ K.-i. Uchida, T. An, Y. Kajiwara, M. Toda, and E. Saitoh, *Applied Physics Letters* **99**, 212501 (2011).